Physics Letters B 811 (2020) 135941

Contents lists available at ScienceDirect

Physics Letters B

www.elsevier.com/locate/physletb

Systematics of the mass-asymmetric fission of excited nuclei from ^{176}Os to ^{206}Pb

E. Prasad [a,*,1], D.J. Hinde [a], M. Dasgupta [a], D.Y. Jeung [a], A.C. Berriman [a], B.M.A. Swinton-Bland [a], C. Simenel [a,b], E.C. Simpson [a], R. Bernard [a,b], E. Williams [a], K.J. Cook [a,2], D.C. Rafferty [a,3], C. Sengupta [a,4], J.F. Smith [a,5], K. Vo-Phuoc [a], J. Walshe [a]

[a] Department of Nuclear Physics, Research School of Physics, Australian National University, Canberra, ACT 2601, Australia
[b] Department of Theoretical Physics, Research School of Physics, Australian National University, Canberra, ACT 2601, Australia

ARTICLE INFO

Article history:
Received 5 August 2020
Received in revised form 4 November 2020
Accepted 5 November 2020
Available online 23 November 2020
Editor: D.F. Geesaman

Keywords:
Nuclear fission
Neutron deficient nuclei
Mass-asymmetric fission
Deformed shell gaps

ABSTRACT

The competition between the dominant mass-asymmetric and rarer narrow mass-symmetric fission modes in actinide nuclei are controlled by deformed and spherical shell effects. The low energy fission of $^{180}_{80}$Hg was recently observed to be strongly mass-asymmetric, indicating that despite spherical shell gaps in fragments around $^{90}_{40}$Zr, the system does not fission mass-symmetrically. Several theoretical approaches have been used to explain this unexpected result.

To investigate the underlying mechanism, systematic measurements of fission mass distributions for isotopes of Os, Pt, Hg and Pb, formed in fusion reactions with p, ^{12}C, ^{32}S, ^{40,48}Ca projectiles, have been made for excitation energies above the fission saddle-point (E^*_{eff}) between 2.8 and 28.2 MeV. Evidence for mass-asymmetric fission is widespread, manifested as flat topped mass distributions or significant deviations from a single Gaussian shape. The systematic trends seen cannot be attributed to quasifission. Comparing two-Gaussian fits at a wide range of E*, it is concluded that the fit centroids reflect the low energy character of mass-asymmetric fission in the sub-lead region.

Quantitative comparisons were made with microscopic calculations by Scamps and Simenel (2019) [33] of fission mass-asymmetries attributed to the influence of shell gaps in both neutrons (N=52, 56 for compact octuple deformations) and protons (Z=34 and Z=42, 44, 46 with large quadrupole deformations). For the predominant fission mode in the calculations, having one elongated and one compact fragment, the results are in extremely good agreement with all experimental values. This provides strong support for both the calculations, and the exploration of mass-asymmetric fission systematics through heavy ion fusion reactions. The total kinetic energy distributions for ^{176}Pt and ^{180}Pt do not show any evidence of a low TKE mass-symmetric fission mode, as had been reported for ^{178}Pt by Tsekhanovich et al. (2019) [39].

Nuclear fission is a large scale collective rearrangement of a microscopic system which involves a subtle interplay of collective and single particle effects. Though fission was discovered [1,2] more than eighty years ago, there are many fundamental questions that are not yet fully understood [3]. Apart from its significance as a fundamental nuclear phenomenon, fission is important in the astrophysical *r* process [4,5], the creation of heavy [6] and medium heavy [7] nuclei, the creation of nuclei far from stability [8], in power production and in the synthesis of radio-isotopes — all these demand a clear understanding of the fission process.

One of the key characteristics of fission is the fragment mass distribution. In the spontaneous and low energy fission of actinide nuclei, the fragment mass division was observed to be asymmetric at the time of discovery, unlike the symmetric mass splits predicted by the liquid drop model [9,10]. An early proposed explanation [10–12] was the extra binding energy of fragments with completely filled spherical proton and neutron shells at Z=50, N=82

* Corresponding author.
E-mail address: prasadenair@cukerala.ac.in (E. Prasad).
[1] Present address: Department of Physics, School of Physical Sciences, Central University of Kerala, Periye -671320, India.
[2] Present address: National Superconducting Cyclotron Laboratory, Michigan State University, East Lansing, MI 48824, USA.
[3] Present address: UK.
[4] Present address: ACRF Image X Institute, University of Sydney, Central Clinical School, Sydney, Australia.
[5] Present address: Advanced Technology Institute, University of Surrey, Guildford, Surrey, GU2 7XH, United Kingdom.

https://doi.org/10.1016/j.physletb.2020.135941

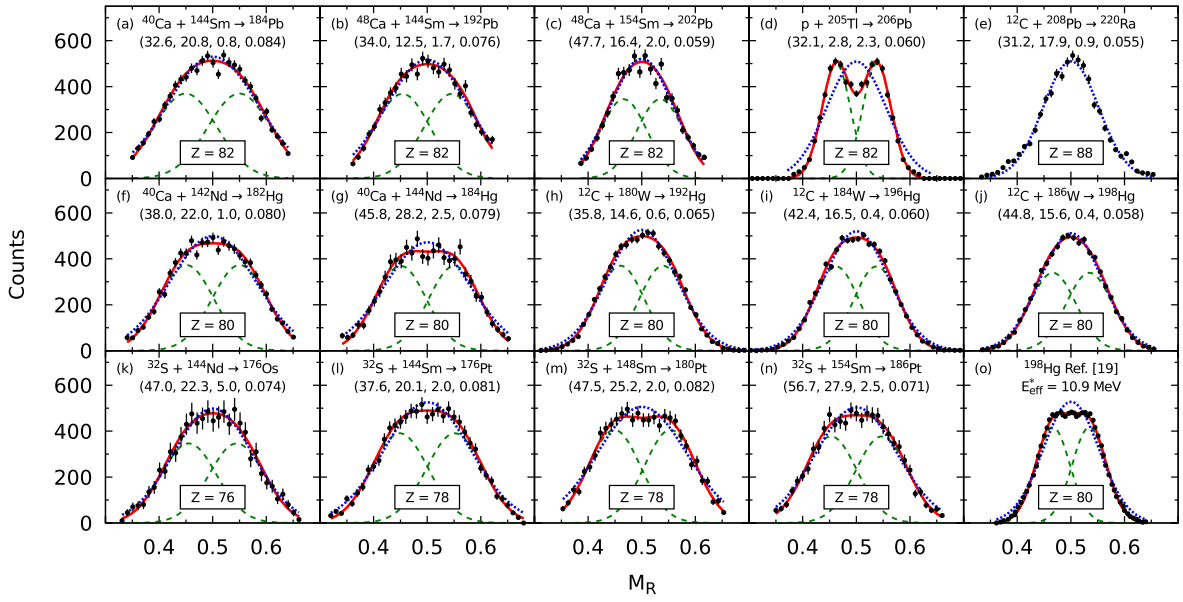

Fig. 1. Fission mass-ratio (M_R) distributions for different nuclei at selected excitation energies E^* (see text). In each panel (in brackets) the E^*, E^*_{eff} (in MeV), the factor scaling the experimental counts, and the single Gaussian fit standard deviation are given. The single Gaussian (dotted blue curve) and two-Gaussian fits (red curve) are shown for each system, with the green dashed curves being the two Gaussian components.

[13]. Further data indicated that fragment yields might be correlated with the deformed neutron shell gap around N=88 [14,15]. Later, a systematic investigation [16] of the charge division in actinide fission suggested that the Z of the heavy fragment (with peak yield around Z=54) is the driver of the dominant mass-asymmetric fission of actinide nuclei. Recently, it has been proposed that this may result from the extra stability of octupole deformations [17] of fragments with Z=52, 56. A transition to mass-symmetric fission is observed with increasing compound nucleus (CN) excitation energy (E*), due to the expected damping of shell effects. A transition to a mass-symmetric peak is also seen with decreasing mass (A) or charge (Z) of the fissioning nucleus below Th [16,18]. For A<220, the fragment mass division was considered to be generally dominated by mass-symmetric fission [19–21].

The discovery that the low energy (β-delayed) fission of ^{180}Hg is markedly mass-asymmetric [22–25] triggered renewed interest in the fission of pre-lead nuclei. The masses were observed to peak at 80(1) and 100(1) u, indicating that spherical shell gaps in fragments around ^{90}Zr do not result in symmetric fission being dominant. Calculations based on a macroscopic-microscopic picture [22,26,27] showed that the features of the potential energy surface in the Mercury region are significantly different to those of the actinide nuclei. It was thus suggested that the mechanism of fission in the actinide and Hg regions are different in nature [26,27]. Shell effects in the pre-scission configuration [28], in particular quadrupole deformed neutron shells in the fragments [29–31], and the coupling between the neutron orbitals of the types [40∧Ω] and [51∧Ω] in the fissioning system [32] were also proposed as explanations.

Most recently microscopic mean-field calculations based on the Hartree-Fock approach with BCS pairing correlations [33] led to the proposal that octupole deformed shell gaps in the fragments may play a significant role in the fission mass-splits of sub-lead nuclei, as had also been proposed in the fission of actinide nuclei [17]. It was also shown that proton shell gaps appear for large quadrupole deformations at Z = 34, and at Z = 42, 44, 46, which may also play an important role [34].

In this Letter, we present extensive new measurements of fission mass distributions for 14 nuclei lighter than ^{208}Pb. The results suggest that proton numbers in the fragments indeed play a major role in the mass-asymmetric fission in sub-lead nuclei.

The experiments were performed at the Heavy Ion Accelerator Facility of the Australian National University. Pulsed heavy ion beams of ^{40,48}Ca, ^{32}S, and ^{12}C with a pulse separation of 107 ns and FWHM of 0.7-1.5 ns were used. Fusion-fission mass distributions for isotopes of Osmium (^{176}Os), Platinum (^{176,180,186}Pt), Mercury (^{182,184,192,196,198}Hg), and Lead (^{184,192,202}Pb) were measured, typically at three beam energies for each reaction. The effective fission excitation energy above the angular momentum dependent fission barrier is defined as $E^*_{eff} = E^* - B_f(\ell) - E_{rot}(\ell) - E_{pre}$ where $B_f(\ell)$ is the angular momentum dependent fission barrier, $E_{rot}(\ell)$ is the rotational energy and E_{pre} is the energy removed by the pre-fission particle emission (see supplemental material). This ranged between 12.5 and 28.2 MeV. The mass distribution was also measured for fission of ^{220}Ra populated at $E^* = 31.2$ MeV using the ^{12}C + ^{208}Pb reaction. Expected to be mass-symmetric [16], this serves as a benchmark for comparison with lighter systems. Fission of ^{206}Pb was measured for the p + ^{205}Tl reaction, at $E^*_{eff} \sim$ 2.8 MeV, where the effect of shell gaps on the mass distribution would be expected to be very strong.

Fission fragments were detected using large area multi-wire proportional counters (MWPCs) [35]. Additional details of the measurement and analysis procedures [35,36] are described in the supplemental material. Analysis using the kinematic coincidence method provides the ratio of the mass of one fragment to the total mass at scission (M_R). The experimental M_R distributions were determined typically within an angular range $90° < \theta_{cm} < 135°$, with constant acceptance in azimuthal angle within that range.

These distributions are shown in Fig. 1(a)–Fig. 1(n). The distributions are not mirrored around mass-symmetry, so represent the raw M_R spectra. For each measurement, values are shown (in brackets) of the CN excitation energy E*, E^*_{eff}, the scaling factor multiplying the experimental counts when plotting the yields, and the σ_{MR} values of single Gaussian fits (dotted blue curves) to each M_R distribution.

The fission mass distribution for the heaviest nucleus ^{220}Ra (Fig. 1(e)) shows a peak at symmetry consistent with a single Gaussian shape, as expected. As the fissioning systems become lighter and more neutron deficient, there is a systematic transition

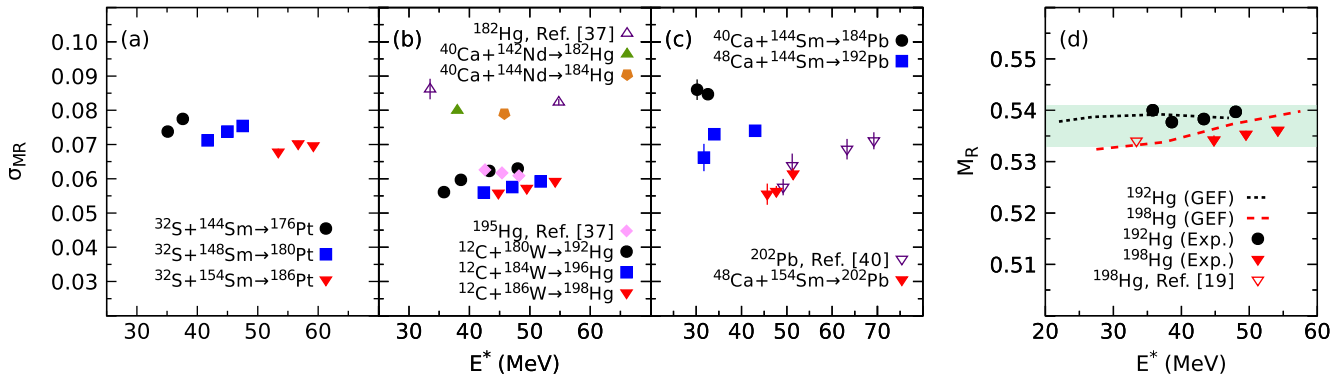

Fig. 2. σ_{MR} of single Gaussian fits to the measured M_R distributions of the isotopes of Pt (panel a), Hg (panel b) and Pb (panel c) as a function of E^*. At similar E^*, the lighter isotopes show larger σ_{MR} values. Panel (d) shows the heavy fragment peak positions from two-Gaussian fits as a function of E^* for ^{192}Hg and ^{198}Hg, from the present work and from Ref. [19]. Two-Gaussian fits to GEF [3] calculations for the same nuclides are shown by dashed curves. The pale green region represents the systematic uncertainty band conservatively assigned to experimental M_R centroids to account for their possible dependence on E^*.

to wider flat-topped distributions. These results are in qualitative agreement with previous heavy ion induced fission data for ^{182}Hg, ^{195}Hg [37], ^{180,190}Hg [38], and ^{178}Pt [39]. As well as the heavy ion induced fission, mass-ratio distributions from proton-induced fission of ^{206}Pb (this work) and ^{198}Hg [19] are shown in Fig. 1(d) and (o). These reactions populate the CN with a E^*_{eff} value lower than 10 MeV, where the mass-asymmetric structure is more pronounced than at the higher E^*_{eff} of the heavy ion induced reactions.

To investigate the systematic nature of the fission mass distributions, the first step in the analysis was to determine the overall mass-width as a function of CN atomic number, mass number and excitation energy, through fitting the distributions by a single Gaussian function. The Gaussian standard deviations σ_{MR} are plotted in Fig. 2(a)-(c) for the isotopes of Pt, Hg, and Pb respectively, as a function of excitation energy of the CN. Within experimental uncertainty, the widths increase with excitation energy as would be expected [19,20]. Widths from previous measurements are also shown (where tabulated) [37,40]. The current results are in good agreement. Furthermore, for each element, the widths show a systematic increase with decreasing neutron number. The dependence on E^* makes quantitative comparisons difficult, given the broad range of measurements. A different approach to investigate the systematics has been taken, as described below.

With heavy ion projectiles ranging from C to Ca, the possible role of quasifission [41,42] in these trends must be considered [37,43]. As in previous measurements for the ^{40}Ca+^{142}Nd reaction [37], no mass-angle correlation in the mass-symmetric region was found (see Supplemental Material), indicating that fast quasifission does not contribute significantly. Evidence for very mass-asymmetric quasifission had been found [40] for the ^{48}Ca+^{154}Sm reaction, but it was concluded that for more mass-symmetric splits, fusion-fission is dominant. As seen in Fig. 2(c) the current widths are in excellent agreement with those tabulated in ref. [40]. It is clear from Fig. 1 and Fig. 2 that this reaction gives the smallest σ_{MR} value of all the sub-Pb measurements. This is the opposite of expectations if the distribution was determined by incomplete mass equilibration as found for *fast* quasifission. If there were a component of *slow* quasifission [44] in the mass-symmetric region, it would be expected to result from trajectories reaching close to or inside the unconditional saddle point [45]. Slow quasifission might thus be expected to experience the same shell structure as fusion-fission whilst moving to scission, and show its influence in the mass spectrum, as found for example in S+Pb reactions [46]. It is concluded that quasifission does not interfere significantly with the observed trends seen in these mass-split distributions.

The single Gaussian fits in general give a poor representation of the M_R spectra. This is particularly evident for the low E^*_{eff} proton induced fission spectrum for ^{206}Pb (Fig. 1(d)), which shows a marked dip in yield at mass-symmetry. This spectrum can be very well represented by two Gaussians with equal heights and widths, having equal but opposite offsets ($\pm\Delta M_R$) from $M_R = 0.5$. The total fit and components are shown by full red and dashed green curves respectively. These mass-asymmetric peaks will result from structure in the potential energy surface resulting from shell effects. With increasing E^*, shell structure is expected to be attenuated. Nevertheless, in the sub-Pb region fission mass distributions for E^* as high as 70.5 MeV [38] have been well-reproduced by the sum of two mass-asymmetric Gaussian peaks: for ^{180,182}Hg, they were consistent with the peak positions seen at low E^* for ^{180}Hg in β-delayed fission [37,38].

The results of two-Gaussian fits to the present data are shown in Fig. 1 by the red curves, which represent all the distributions very well. Compared to the single Gaussian fits, in many cases the improved fit quality is very clear. In others, the difference is less obvious, being similar to the size of the statistical error bar on an individual data point. It is well-known that a single Gaussian distribution can be well-represented by two Gaussians, but the additional degree of freedom compared to a single Gaussian should permit a better fit. It was thus crucial to carefully determine the statistical uncertainty in the deduced centroids. To do this the total χ^2 as a function of ΔM_R was evaluated, with the Gaussian common widths and heights unconstrained. Examples are shown in Fig. 2 of the Supplemental Material. The lowest value of χ^2 gives the optimum value of ΔM_R, and the statistical uncertainty comes from the higher and lower values of ΔM_R where χ^2 exceeds the minimum value by one. The extracted values of ΔM_R in general have very high statistical significance, with typical values of $\Delta M_R = 0.045 \pm 0.001$. For the benchmark ^{220}Rn fission, the fit gave $\Delta M_R = 0.000 \pm 0.013$, a result favouring a single Gaussian peak.

A further critical question must be answered before interpreting the two-Gaussian fit centroids in terms of the underlying physics. Do these mass centroids from heavy-ion fusion-fission mass distributions correspond to the positions of the underlying mass-asymmetric valleys in the potential energy surface? Two approaches have been taken to address this question.

The first is from the information carried by the experimental data alone. Existing evidence from fits to the flat-topped distributions for light Hg isotopes [37,38] are here extended to fission of more neutron-rich Hg isotopes, where the signature of asymmetric fission in the distributions is weaker. The peak positions in M_R of the heavy fragment Gaussian as a function of E^* are presented in Fig. 2(d), for fission of ^{192,198}Hg following the ^{12}C + ^{180,186}W and p + ^{197}Au [19] fusion reactions. The heavy-ion reaction centroids

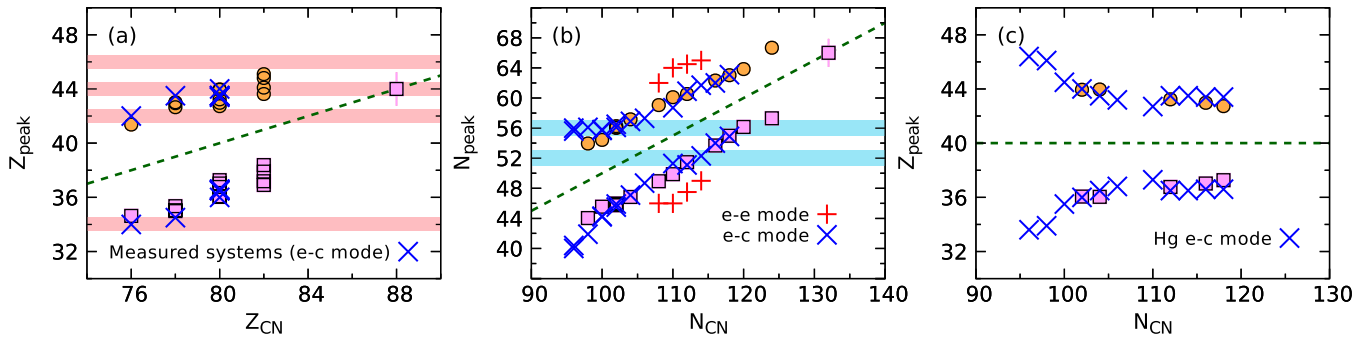

Fig. 3. Panel (a) shows light (squares) and heavy (circles) fragment Z_{peak} as a function of Z_{CN}, whilst (b) and (c) respectively show fragment N_{peak} and Z_{peak} as a function of N_{CN}. The dashed green lines show the expectations for symmetric fission. Z_{peak} values in (a) correlate with expected proton shell gaps (pink bands) at Z=34 (light fragments), and 42, 44 and 46 (heavy fragments). The crosses show the predictions of Scamps et al. [33,34] for the same systems (±2 neutrons), for the elongated-compact (e-c) fission mode. These predictions agree very well with the experimental values. N_{peak} values in (b) show a uniform distribution with N_{CN}. The calculated results [33,34] for two fission modes, having either elongated and compact fragments (e-c) or two elongated fragments (e-e), are shown by blue and red crosses respectively (see text). Most systems have a light or heavy fragment in the region of octupole deformed neutron shell gaps at N=52, 56 (blue bands). In (c) fission of different isotopes of Hg match closely with the calculated values for the elongated-compact fission mode.

are almost independent of E*, and for ^{198}Hg they agree very well with the peak position at the lowest E* from proton-induced fission. This indicates empirically that the Gaussian fits to the higher E* distributions carry equivalent information as at low E*.

The second approach made use of model calculations with GEF [47,3], as a function of E* for ^{192}Hg and ^{198}Hg. These predict increasingly pronounced mass-asymmetric features as E* is decreased. The two-Gaussian fits to the GEF calculated mass distributions return centroids that change very little with E*, remaining close to the centroids of the well-defined mass-asymmetric peaks at low E*, as shown by the dashed lines in Fig. 2(d). These observations of the stability of the two-Gaussian fit peak positions provide a platform to extract quantitative information from the mass distributions, and compare results from different reactions and excitation energies in a way that cannot be achieved with the widths of single Gaussian fits.

In the subsequent analysis of the extracted mass-asymmetric peak centroids we have conservatively added in quadrature with the purely statistical uncertainty in ΔM_R a systematic uncertainty of ±0.004, indicated in Fig. 2(d) by the pale green band. This accounts for the possible slow dependence of the centroids on E*, since the experimental M_R spectra for the different nuclides cover a range of E*.

Concluding that the empirical two-Gaussian fit centroids are related to the positions of the mass-asymmetric fission valleys, the optimum experimental conditions to determine the centroids must be chosen. The increased sensitivity of the mass distributions to shell structure at the lowest E* has to be balanced against the reduction in statistics arising from exponentially falling fission cross sections with reducing beam energy. A compromise between these two considerations was made in selecting the excitation energies of the data shown in Fig. 1 and used in the subsequent investigation of systematic behaviour of the mass-asymmetric fission characteristics.

To relate the positions of the extracted peaks in M_R to shell structure, their positions must be converted to the fission fragment proton and neutron numbers at scission. Two standard assumptions were made, that the mass at scission is that of the CN, and that the N/Z ratios of the fragment are those of the CN. Thus for a Gaussian peak centroid at M_R, the corresponding fragment peak positions in Z and N are $Z_{peak} = M_R \times Z_{CN}$ and $N_{peak} = M_R \times N_{CN}$.

The extracted values of Z_{peak} and N_{peak} are shown as a function of Z_{CN} and N_{CN} in Fig. 3(a) and Fig. 3(b), (c), respectively. The values are also tabulated in the supplemental material. The effect of pre-fission neutron emission is small as described in the supplemental material.

The experimental values of Z_{peak} shown as a function of Z_{CN} in Fig. 3(a) deviate significantly from the expectation for mass-symmetric division (shown by the dashed line) except for ^{220}Ra. For all systems, including ^{220}Ra, the peaks are in the regions $34<Z_{peak}<38$ and/or $42<Z_{peak}<46$. Microscopic model calculations in the sub-Pb region [33] found proton shell gaps (expected to result in valleys in the potential energy surface) at Z=34 and 42, 44, 46, indicated by the pink bands. These gaps are found at large quadrupole deformations ($\beta_2 = 0.6$ to 1.0), which may be consistent with fragment deformations near scission. The experimental data seem to be correlated with one or both of these shell gaps. The calculated [33] most likely asymmetric fission masses for the measured systems (±2 neutrons) are shown by crosses. The agreement is excellent.

Where shell gaps in both fragments are present for the same mass or charge split, it is likely that the effect on the mass distribution will be stronger than when present in only one fragment. Because of the parabolic dependence of the liquid drop potential energy on mass or charge ratio, shell gaps nearer to symmetric splits will have more effect than those further away. For these reasons, it may be that for Os ($Z_{CN} = 76$), the shell gap at Z=34 plays a large role, being quite close to mass-symmetry. As Z_{CN} increases, the Z=34 gap moves further away, whilst the Z=42, 44, 46 gaps move closer to symmetry, and so should have the stronger effect on the mass distribution. Finally, by $Z_{CN} = 88$, these gaps may reinforce the liquid drop potential, strongly favouring symmetric fission.

Ref. [33] highlights the importance of neutron shell gaps at more compact octupole deformations around N = 52 and 56 (blue bands in Fig. 3(b)). The extracted experimental values of N_{peak} as a function of N_{CN} are shown. In contrast to Z_{peak}, the N_{peak} values are smoothly distributed as a function of N_{CN}, showing no apparent bunching, or avoidance, in any particular range of N_{peak}. However, the calculated N_{peak} values (blue crosses) are in extraordinarily good agreement above N_{CN} =102. Below this value they are constant at N=56, but unfortunately experiment does not extend to low enough N_{CN} values to really test this behaviour. The blue crosses all correspond to one elongated fragment with large quadrupole deformation, the other having a more compact octupole shape [34]. There is a group of points (red crosses) in the middle of the N_{CN} range that lie at larger asymmetries. These correspond to a calculated second fission mode having both fragments with large quadrupole deformation. Although the data cannot resolve modes closely spaced in mass, the agreement of the exper-

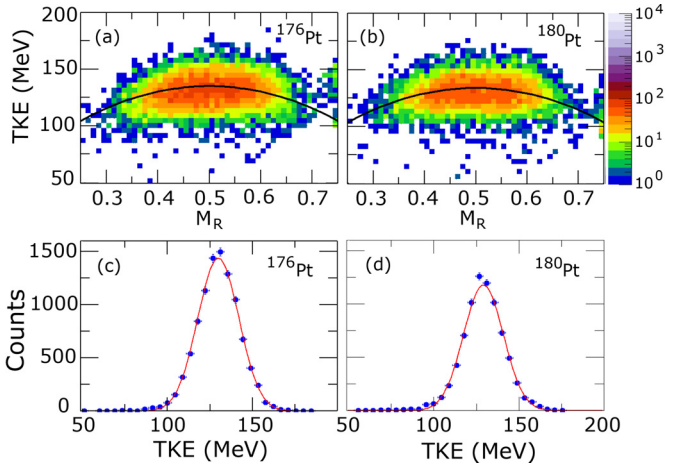

Fig. 4. Panels (a,b) show mass-ratio vs TKE for fission of ^{176}Pt and ^{180}Pt. The counts scale is on the right. The black curves show the expectations based on Viola fission TKE systematics (see text). The fission TKE distributions are shown in (c,d), with Gaussian fits in red emphasising the absence of a strong low TKE tail previously reported [39] for ^{178}Pt.

imental (average) asymmetry with the quadrupole-octupole mode suggests that the calculated elongated-elongated mode has a significantly lower probability.

To further probe the role of neutrons, Z_{peak} is shown as a function of N_{CN} in Fig. 3(c) for isotopes of Hg. Experimentally there is a weak dependence of Z_{peak} on neutron number, with the mass-asymmetry consistently reducing as N_{CN} increases. Similar behaviour is seen for Pt and Pb isotopes. This trend agrees very well with the calculations for the elongated-compact mode in Hg isotopes (blue crosses). Future fission measurements determining both Z and N of the fragments [18] would give further insights into the relative influence of different shell gaps on mass-asymmetric fission in this mass region.

The mass distribution is one of the key fission observables. Another is the total kinetic energy (TKE) of the fission fragments, which is related to the elongation of the system at scission. Measurements [38] in the sub-Pb region have found the TKE to be slightly lower than expectations based on the Viola systematics [48] that parameterises a wide range of measured mean TKEs spanning the chart of the nuclides. However, a recent measurement for ^{36}Ar + ^{142}Nd forming ^{178}Pt found a remarkable result [39]. As well a flat-topped mass distribution with mean TKE consistent with previous measurements in this region, a *mass-symmetric* mode with *low* TKE also was seen in the experiment. This was attributed to a very elongated scission configuration, and taken as evidence for multimodal fission in the sub-Pb mass region [39].

In this work, we have not studied ^{178}Pt, but have made measurements for ^{176}Pt and ^{180}Pt *via* the ^{32}S + ^{144,148}Sm fusion reactions. As well as the mass-ratios, the TKE was determined event-by-event using the same kinematic coincidence method as Ref. [39]. M_R vs. TKE spectra are shown for the range $0.25 < M_R < 0.75$ in Fig. 4 for these two systems. The curved lines represent the expected dependence of TKE on M_R, based on the Viola systematics [49]. No evidence for a mass-symmetric low TKE fission mode is seen. The TKE distributions for all fission events are shown in Fig. 4(c), (d). These are essentially symmetric, each well-represented by a single Gaussian distribution (red curves), with no detectable low TKE component, unlike the 30% contribution seen [39] for ^{178}Pt.

Detector system resolution effects could not cause the elimination of such a strong group of events seen for ^{178}Pt. It is concluded that this difference must be attributed to the different compound nucleus, the different projectile or the different target. The physics underlying this difference is currently not known. It would be valuable to form the same ^{178}Pt compound nucleus by another reaction to investigate whether this is an extremely localised phenomenon. It would also be of interest to see whether theoretical calculations [39] might predict different behaviour for the neighbouring ^{176}Pt and ^{180}Pt nuclei.

In summary, fission mass distributions of 14 nuclides between ^{176}Os and ^{206}Pb, formed in a range of fusion reactions, have all been found to show strong evidence of mass-asymmetric fission. For a wide range of excitation energy (33 MeV $< E^* <$ 54 MeV for ^{198}Hg, refer Fig. 2(d)) the mass centroids from two-Gaussian fits do not change, indicating that they reflect the position of shell structure in the fission potential energy surface. The deduced proton centroids Z_{peak} correspond closely to calculated [33] proton shell gaps for large quadrupole deformations at Z=34 and Z=42, 44, 46. The deduced neutron centroids N_{peak} are uniformly distributed, with no obvious signature of the octupole deformed neutron shell gaps at N=52, 56 [33]. Nevertheless the calculated values of both Z_{peak} and N_{peak} (for the predominant calculated fission mode with elongated quadrupole and compact octupole fragment deformations) are in extremely good agreement with all experimental values, providing strong support for both the calculations, and for the exploration of mass-asymmetric fission systematics through heavy ion fusion reactions. The unexpected low TKE mass-symmetric fission mode reported [39] for fission of ^{178}Pt has not been observed in the current measurements for ^{176}Pt and ^{180}Pt. Along these lines, the recent work reported by Mahata et al., [50] must be mentioned. Comparing experimental and theoretical results, they concluded that proton shells are dominant in determining the fission mass distributions of neutron-deficient nuclei around lead. Further experimental and theoretical investigation is called for.

Declaration of competing interest

The authors declare that they have no known competing financial interests or personal relationships that could have appeared to influence the work reported in this paper.

Acknowledgements

The authors are grateful for support from the Australian Research Council through grants DP160101254, DP200100601 and DP190100256. Support for HIAF accelerator operations through the HIA capability of the Federal Government NCRIS program is acknowledged.

Appendix A. Supplementary material

Supplementary material related to this article can be found online at https://doi.org/10.1016/j.physletb.2020.135941.

References

[1] O. Hahn, F. Strassman, Naturwissenschaften 27 (1939) 11.
[2] L. Meitner, O.R. Frisch, Nature 143 (1939) 239.
[3] K.-H. Schmidt, B. Jurado, Rep. Prog. Phys. 81 (2018) 106301.
[4] I. Panov, E. Kolbe, B. Pfeiffer, T. Rauscher, K.-L. Kratz, F.-K. Thielemann, Nucl. Phys. A 747 (2005) 633.
[5] I. Petermann, K. Langanke, G. Martínez-Pinedo, I. Panov, P.G. Reinhard, F.K. Thielemann, Eur. Phys. J. A 48 (2012) 122.
[6] P. Armbruster, Rep. Prog. Phys. 62 (1999) 465.
[7] C-O. Wene, S.A.E. Johansson, Phys. Scr. 10 (1974) 156.
[8] E. Kugler, Hyperfine Interact. 129 (2000) 23.
[9] N. Bohr, J.A. Wheeler, Phys. Rev. 56 (1939) 426.
[10] L. Meitner, Nature 165 (1950) 561.
[11] M.G. Mayer, Phys. Rev. 74 (1948) 235.
[12] R. Vandenbosch, J.R. Huizenga, Nuclear Fission, Academic, New York, 1973.
[13] M.G. Mayer, Phys. Rev. 78 (1950) 22.

[14] B.D. Wilkins, E.P. Steinberg, R.R. Chasman, Phys. Rev. C 14 (1976) 1832.
[15] C. Gustafsson, P. Möller, S. Nilsson, Phys. Lett. B 34 (1971) 349.
[16] K-H. Schmidt, S. Steinhäuser, C. Böckstiegel, A. Grewe, A. Heinz, A.R. Junghans, J. Benlliure, H-G. Clerc, M. de Jong, J. Müller, M. Pfützner, B. Voss, Nucl. Phys. A 665 (2000) 221.
[17] G. Scamps, C. Simenel, Nature 564 (2018) 382.
[18] A. Chatillon, et al., Phys. Rev. C 99 (2019) 054628.
[19] M.G. Itkis, V.N. Okolovich, G.N. Smirenkin, Nucl. Phys. A 502 (1989) 243c.
[20] M.G. Itkis, V.N. Okolovich, A.Ya. Rusanov, G.N. Smirenkin, Z. Phys. A 320 (1985) 433.
[21] V.V. Pashkevich, Nucl. Phys. A 169 (1971) 275.
[22] A.N. Andreyev, J. Elseviers, M. Huyse, P. Van Duppen, S. Antalic, A. Barzakh, N. Bree, T.E. Cocolios, V.F. Comas, J. Diriken, et al., Phys. Rev. Lett. 105 (2010) 252502.
[23] A.N. Andreyev, M. Huyse, P. Van Duppen, Rev. Mod. Phys. 85 (2013) 1541.
[24] J. Elseviers, A.N. Andreyev, M. Huyse, P. Van Duppen, S. Antalic, A. Barzakh, N. Bree, T.E. Cocolios, V.F. Comas, J. Diriken, et al., Phys. Rev. C 88 (2013) 044321.
[25] V. Liberati, A.N. Andreyev, S. Antalic, A. Barzakh, T.E. Cocolios, J. Elseviers, D. Fedorov, V.N. Fedoseeev, M. Huyse, D.T. Joss, et al., Phys. Rev. C 88 (2013) 044322.
[26] T. Ichikawa, A. Iwamoto, P. Möller, A.J. Sierk, Phys. Rev. C 86 (2012) 024610.
[27] P. Möller, J. Randrup, A.J. Sierk, Phys. Rev. C 85 (2012) 024306.
[28] S. Panebianco, J.-L. Sida, H. Goutte, J.-F. Lemaître, N. Dubray, S. Hilaire, Phys. Rev. C 86 (2012) 064601.
[29] A.V. Andreev, G.G. Adamian, N.V. Antonenko, Phys. Rev. C 86 (2012) 044315.
[30] A.V. Andreev, G.G. Adamian, N.V. Antonenko, A.N. Andreyev, Phys. Rev. C 88 (2013) 047604.
[31] A.N. Andreev, G.G. Adamian, N.V. Antonenko, Phys. Rev. C 93 (2016) 034620.
[32] T. Ichikawa, P. Möller, Phys. Lett. B 789 (2019) 679.
[33] G. Scamps, C. Simenel, Phys. Rev. C 100 (2019) 041602(R).
[34] G. Scamps, C. Simenel, Supplemental material, Phys. Rev. C 100 (2019) 041602(R).
[35] D.J. Hinde, M. Dasgupta, J.R. Leigh, J.C. Mein, C.R. Morton, J.O. Newton, H. Timmers, Phys. Rev. C 53 (1996) 1290.
[36] R. du Rietz, E. Williams, D.J. Hinde, M. Dasgupta, M. Evers, C.J. Lin, D.H. Luong, C. Simenel, A. Wakhle, Phys. Rev. C 88 (2013) 054618.
[37] E. Prasad, D.J. Hinde, K. Ramachandran, E. Williams, M. Dasgupta, I.P. Carter, K.J. Cook, D.Y. Jeung, D.H. Luong, S. McNeil, C.S. Palshetkar, D.C. Rafferty, C. Simenel, A. Wakhle, J. Khuyagbaatar, Ch.E. Düllmann, B. Lommel, B. Kindler, Phys. Rev. C 91 (2015) 064605.
[38] K. Nishio, A.N. Andreyev, R. Chapman, X. Derkx, Ch.E. Düllmann, L. Ghys, F.P. Heßberger, K. Hirose, H. Ikezoe, J. Khuyagbaatar, B. Kindler, B. Lommel, H. Makii, I. Nishinaka, T. Ohtsuki, S.D. Pain, R. Sagiadak, I. Tsekhanovich, M. Venhart, Y. Wakabayashi, S. Yan, Phys. Lett. B 748 (2015) 89.
[39] I. Tsekhanovich, A.N. Andreyev, K. Nishio, D. Denis-Petit, K. Hirose, H. Makii, Z. Matheson, K. Morimoto, K. Morita, W. Nazarewicz, R. Orlandi, J. Sadhukhan, T. Tanaka, M. Vermeulen, M. Warda, Phys. Lett. B 790 (2019) 583.
[40] G.N. Knyazheva, E.M. Kozulin, R.N. Sagaidak, A.Yu. Chizhov, M.G. Itkis, N.A. Kondratiev, V.M. Vorkressensky, A.M. Stefanini, B.R. Behera, L. Corradi, E. Fioretto, A. Gadea, A. Latina, S. Szilner, M. Troatta, S. Beghini, G. Montagnoli, F. Scarlassara, F. Hass, N. Rowley, P.R.S. Gomes, A. Szanto de Toledo, Phys. Rev. C 75 (2008) 064602.
[41] J.P. Blocki, H. Feldmeier, W.J. Świateck, Nucl. Phys. A 459 (1986) 145.
[42] W.J. Światecki, Phys. Scr. 24 (1981) 113.
[43] R. Tripathi, et al., Phys. Rev. C 92 (2015) 024610.
[44] D.J. Hinde, D.Y. Jeung, E. Prasad, A. Wakhle, M. Dasgupta, M. Evers, D.H. Luong, R. du Rietz, C. Simenel, E.C. Simpson, E. Williams, Phys. Rev. C 97 (2018) 024616.
[45] Y. Aritomo, M. Ohta, Nucl. Phys. A 744 (2004) 3.
[46] J. Khuyagbaatar, D.J. Hinde, I.P. Carter, M. Dasgupta, Ch.E. Düllmann, M. Evers, D.H. Luong, R. du Rietz, A. Wakhle, E. Williams, A. Yakushev, Phys. Rev. C 91 (2015) 054608.
[47] K.-H. Schmidt, B. Jurado, C. Amouroux, C. Schmitt, Nucl. Data Sheets 131 (2016) 107.
[48] V.E. Viola, K. Kwiatkowski, M. Walker, Phys. Rev. C 31 (1985) 1550.
[49] J. Toke, R. Bock, G.X. Dai, A. Gobbi, S. Gralla, K.D. Hildenbrand, J. Kuzminski, W.F.J. Müller, A. Olmi, H. Stelzer, B.B. Back, S. Bjørnholm, Nucl. Phys. A 440 (1985) 327.
[50] K. Mahata, et al., https://arxiv.org/abs/2007.16184 [nucl-th].